DOI: 10.24874/ti.2190.04.26.06

Tribology in Industry

www.tribology.rs

RESEARCH

Composition-Dependent Stability and Tribological Performance of Biodiesel-Derived Hybrid TiO_2/MoS_2 Tribofluids Based on a Peltophorum pterocarpum and Waste Cooking Oil Methyl Ester Blend

T. Dayananda Murthy[a,*], H. Yogish[a], N.S. Kumaraswamy[a], R. Pavankumar[a]

[a]*Department of Mechanical Engineering, SJCE, JSS Science and Technology University, Mysore, India.*

Keywords:

Biodiesel tribofluid
TiO_2/MoS_2 hybrid nanoparticles
Peltophorum pterocarpum
Waste cooking oil
Dispersion stability
Four-ball tribology
Wear reduction

* Corresponding author:

Dayananda Murthy T
E-mail:
dayanandamurthy21@gmail.com

Received: 23 April 2026
Revised: 15 May 2026
Accepted: 1 June 2026

A B S T R A C T

This study evaluates TiO_2-, MoS_2-, and hybrid TiO_2/MoS_2 nanoparticles as additives for a characterized 50:50 Peltophorum pterocarpum methyl ester:waste cooking oil methyl ester base fluid. The base fluid was dominated by methyl oleate, methyl linoleate, and methyl palmitate and had an acid number of 0.27 mg KOH/g, water content of 318 mg/kg, and oxidation stability of 4.7 h. A two-stage design screened additives at 0.05 wt.% and then optimized the 25:75 TiO_2:MoS_2 hybrid from 0.025 to 0.10 wt.%. Tribofluids with 0.20 wt.% Span 80 were assessed by density, viscosity, apparent zeta potential, sedimentation, four-ball testing, and SEM/EDS. The 0.05 wt.% 25:75 hybrid gave the best batch-specific response, with apparent zeta potential of −45.7 ± 1.1 mV, 60 d sedimentation index of 2.5 ± 0.2%, coefficient of friction of 0.049 ± 0.001, wear scar diameter of 0.51 ± 0.01 mm, and comparative wear-rate index of 3.10 ± 0.08 × 10^{-6} mm^3/N·m. Friction, wear scar diameter, and wear-rate index decreased by 43.0%, 28.2%, and 40.4% relative to the base fluid. SEM/EDS indicated smoother tracks and more uniform Ti/Mo/S-associated signals than the overloaded 0.10 wt.% formulation. The optimum applies to this batch and preparation route.

1. INTRODUCTION

Tribology affects machine efficiency, component life, maintenance intervals, and life-cycle cost. It is also relevant to sustainability because friction and wear are major sources of energy loss, material loss, and lubricant consumption. Green tribology therefore seeks low-friction, low-wear contacts while reducing toxicity, improving biodegradability, and supporting circular-economy feedstock use [1-4].

Vegetable oils, fatty-acid methyl esters, and chemically modified triglycerides are attractive renewable lubricant candidates because polar ester groups can adsorb on metallic surfaces and

improve boundary lubrication. Their practical use is still restricted by oxidative degradation, thermal instability, cold-flow limitations, and insufficient anti-wear performance under severe boundary contacts [1,4-8].

Feedstock selection is therefore important. Waste cooking oil provides a waste-to-value route, while non-edible seed oils avoid direct competition with food resources and diversify renewable feedstocks [6,9]. Peltophorum pterocarpum oil has recently been reported as a potential non-edible biodiesel feedstock after transesterification [10]. A 50:50 PPME:WCOME blend is consequently a useful model base fluid that combines a non-edible methyl ester with a waste-derived methyl ester.

Nanoparticle additives provide a second route to performance improvement. TiO_2 nanoparticles are commonly associated with load support, surface smoothing, and mending-type effects, while MoS_2 is valued for its layered low-shear structure [11-13]. Hybrid TiO_2/MoS_2 systems may combine these functions, but the benefit depends strongly on particle ratio, total loading, dispersion state, and the ability of particles to enter the contact without forming abrasive agglomerates [14,15].

Dispersion stability was therefore treated as a performance variable rather than as a separate formulation issue. In non-aqueous media, however, electrophoretic light-scattering outputs are sensitive to the measurement protocol, medium properties, dilution, and electrokinetic model. For this reason, the zeta-potential values in this manuscript are reported as apparent values for internal comparison only and are interpreted together with sedimentation behavior and tribological results [16].

The objective was to identify a batch-specific TiO_2/MoS_2 ratio and loading that improves the storage stability and four-ball tribological behavior of the PPME:WCOME base fluid without substantially changing density or high-temperature kinematic viscosity. The formulation matrix is given in Table 1, the experimental route is shown in Figure 1, and Tables 2-7 and Figures 2-6 are used to connect formulation, stability, physicochemical behavior, friction/wear response, and SEM/EDS evidence. The base blend was chemically characterized to support reproducibility; however, the results are still not presented as a universal optimum because only one PPME:WCOME batch and one tribological condition were tested.

2. MATERIALS AND METHODS

2.1 Materials, feedstocks, and base-fluid preparation

Peltophorum pterocarpum oil was extracted in the laboratory from validated seeds, and waste cooking oil was collected locally and pretreated before conversion. Methanol, KOH, sulfuric acid, distilled/deionized water, Span 80, and analytical-grade cleaning solvents were used for transesterification, formulation, and specimen preparation. The solid additives were TiO_2 nanoparticles (30-50 nm, 99.9% purity) and MoS_2 nanoparticles (approximately 50 nm, 99.9% purity). Figure 1 summarizes the workflow from feedstock processing to surface analysis, and Table 1 lists the formulation matrix.

Both feedstocks were converted to methyl esters by alkaline transesterification, which is widely used for vegetable-oil and waste-oil conversion to renewable lubricating fluids [6,9,10]. For WCO pretreatment, the collected oil was filtered through a 25 micrometre stainless-steel filter and fine filter paper and then dried at 105 °C for 60 min to remove suspended matter and residual moisture. Transesterification was carried out at an oil:methanol molar ratio of 1:6 using KOH at 1.0 wt.% of oil, 60 °C reaction temperature, 60 min reaction time, and 600 rpm stirring. After phase separation for 12 h, the ester layer was washed with warm distilled water to neutrality and dried at 105 °C for 30 min. The base fluid used throughout the study was a 50:50 PPME:WCOME blend by volume.

The final 50:50 PPME:WCOME base blend was characterized before tribofluid preparation to address base-fluid reproducibility. GC-FID normalized area analysis showed methyl oleate (C18:1) as the dominant FAME (46.8 ± 0.8 area %), followed by methyl linoleate (C18:2; 26.1 ± 0.7 area %) and methyl palmitate (C16:0; 16.9 ± 0.5 area %). Methyl stearate (C18:0; 5.4 ± 0.3 area %), methyl linolenate (C18:3; 1.0 ± 0.1 area %), methyl palmitoleate (C16:1; 0.8 ± 0.1 area %), methyl arachidate (C20:0; 0.6 ± 0.1 area %), methyl eicosenoate (C20:1; 0.4 ± 0.1 area %), and methyl myristate (C14:0; 0.3 ± 0.1 area %) were present as smaller fractions. The overall composition comprised 23.2% saturated, 48.0% monounsaturated, and 27.1% polyunsaturated FAMEs.

Initial fuel-quality indices for the base blend were acid number 0.27 ± 0.02 mg KOH/g, water content 318 ± 18 mg/kg, oxidation stability induction period 4.7 ± 0.2 h at 110 °C, peroxide value 6.4 ± 0.5 meq O_2/kg, and GC-FID ester purity 96.8 ± 0.6 wt.%. Acid number was determined by potentiometric titration, water content by Karl Fischer titration, and oxidation stability by the EN 14112 Rancimat method.

Base-blend quality changed during storage. From 0 to 180 d, acid number increased from 0.27 ± 0.02 to 0.51 ± 0.04 mg KOH/g, water content increased from 318 ± 18 to 430 ± 28 mg/kg, oxidation stability decreased from 4.7 ± 0.2 to 3.3 ± 0.2 h, and peroxide value increased from 6.4 ± 0.5 to 13.6 ± 1.0 meq O_2/kg. These data reduce the reproducibility gap raised by the reviewers, but the reported 0.05 wt.% H2575 response remains batch-specific because tribological validation was conducted on this characterized base-fluid batch and not across multiple independently aged batches.

2.2 Tribofluid formulation and optimization strategy

Span 80 was used as a non-ionic surfactant at a constant 0.20 wt.% of the total formulation so that nanoparticle ratio and total loading remained the primary variables. Each formulation was magnetically stirred at 1000 rpm for 30 min before sonication. Probe sonication was performed using a typical laboratory ultrasonic processor equipped with a titanium alloy probe tip of approximately 12-13 mm diameter. The probe immersion depth was maintained at approximately 15-20 mm below the fluid surface to ensure uniform cavitation and minimize vortex formation. Sonication was conducted at 400 W and 40% amplitude for 30 min under ice-bath cooling using intermittent pulsed operation (5 s ON / 5 s OFF; 50% duty cycle) in a cylindrical borosilicate glass vessel while maintaining the sample temperature below 35 °C. Based on the set power, amplitude setting, and the 900 s effective ON time within the 30 min pulsed treatment, this corresponds to a setting-based nominal ON-time energy estimate of approximately 144 kJ per batch (400 W × 0.40 × 900 s). This value should not be interpreted as the exact acoustic energy delivered to the fluid, because no calorimetric sonication-energy measurement was archived. All formulations in the present comparison were prepared using the same controlled setting-based sonication window.

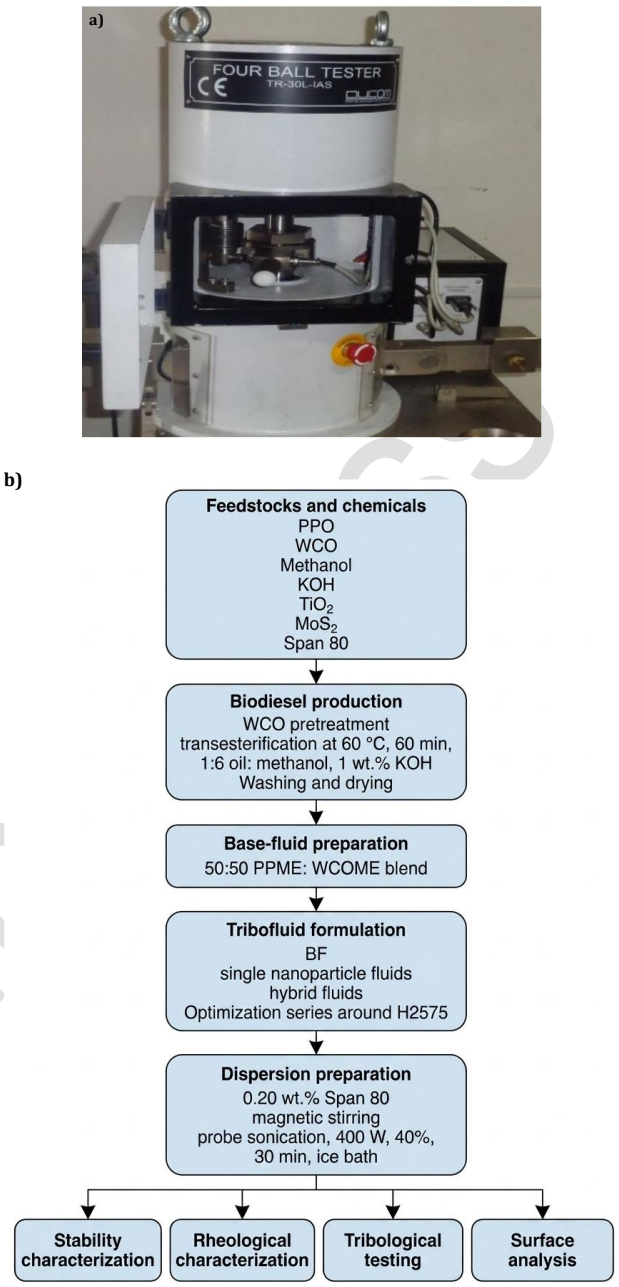

Fig. 1. Experimental methodology: (a) four-ball tribotester used in the present study and (b) workflow from feedstock processing and methyl-ester preparation to tribofluid formulation, characterization, tribological testing, and post-test surface analysis.

A two-stage strategy separated composition screening from loading optimization. In Stage I, TiO_2, MoS_2, and TiO_2/MoS_2 hybrids with 75:25, 50:50, and 25:75 mass ratios were compared at 0.05 wt.% total additive loading. In Stage II, the best Stage I ratio was held constant and the total loading was varied from 0.025 to 0.100 wt.%. The overlap between H2575 and H2575-0050 denotes the same nominal 25:75 hybrid at 0.05 wt.% but preserves the distinction between the screening and loading-optimization batches.

Table 1. Final formulation matrix used for screening and loading optimization of TiO_2-, MoS_2-, and hybrid TiO_2/MoS_2 biodiesel-derived tribofluids.

Sample	Base fluid	Additive (wt.%)	TiO_2 (%)	MoS_2 (%)	TiO_2:MoS_2
BF	50:50 PPME:WCOME	0.000	0	0	-
T05	50:50 PPME:WCOME	0.050	100	0	100:0
M05	50:50 PPME:WCOME	0.050	0	100	0:100
H7525	50:50 PPME:WCOME	0.050	75	25	75:25
H5050	50:50 PPME:WCOME	0.050	50	50	50:50
H2575	50:50 PPME:WCOME	0.050	25	75	25:75
H2575-0025	50:50 PPME:WCOME	0.025	25	75	25:75
H2575-0050	50:50 PPME:WCOME	0.050	25	75	25:75
H2575-0075	50:50 PPME:WCOME	0.075	25	75	25:75
H2575-0100	50:50 PPME:WCOME	0.100	25	75	25:75

2.3 Stability, physicochemical characterization, and rheology

Stability evaluation combined apparent electrokinetic behavior with direct macroscopic settling. Samples were stored at 25 ± 2 °C and examined at 0, 1, 7, 15, 30, and 60 d. Sedimentation index was calculated as SI (%) = (Hs/Ht) × 100, where Hs is sediment height and Ht is total sample height. Fresh aliquots were also examined by UV-Vis at 600 nm. For electrophoretic light-scattering analysis, fresh aliquots were analyzed at 25 ± 1 °C after dilution with the corresponding base-fluid medium at approximately 1:100 volume ratio to minimize multiple scattering effects. Instrument inputs were set using dielectric constant values of approximately 3.1-3.3, refractive index values of 1.45-1.47, and dynamic viscosity corresponding to the measured base-fluid viscosity at the test temperature. The Smoluchowski electrokinetic approximation was used for comparative analysis. Therefore, report apparent zeta-potential values intended primarily for internal ranking within this formulation series [16].

Density at 40 °C was determined according to ASTM D4052 [17], whereas kinematic viscosity at 40 °C and 100 °C was measured in accordance with ASTM D445 [18]. Because all measured KV at 100 °C values were below 2.0 mm^2/s, ASTM D2270-24 does not apply to these fluids and viscosity index was therefore not reported [19]. Flow-curve data were analyzed over a shear-rate range of 10-1000 s^{-1} using Newtonian, power-law, and Herschel-Bulkley fits, and the best model was selected from R^2 and RMSE criteria.

2.4 Tribological testing, wear-rate calculation, and surface analysis

Tribological performance was evaluated using a four-ball tribotester under wear-preventive conditions adapted from ASTM D4172 [20]. As shown in Figure 1a, three fixed lower AISI 52100 steel balls supported a rotating upper ball under a normal load of 392 N. The test speed was 1200 rpm, lubricant temperature was 75 °C, test duration was 60 min, and lubricant volume was 10 mL per run. The balls had a diameter of 12.7 mm, hardness of 64-66 HRC, and surface roughness Ra ≤ 0.05 micrometre. Runs were randomized, each run used fresh lubricant, and the balls were cleaned with acetone and isopropyl alcohol before testing. The coefficient of friction was recorded by the tribotester software from the measured friction/torque signal and reported as the mean value for each run. All tests were performed under identical ASTM D4172-type conditions using the same instrument setup, load, speed, temperature, duration, ball material, lubricant volume, and cleaning procedure. The COF values are therefore interpreted as comparative mean endpoints for ranking the formulations within the present test matrix.

The primary tribological endpoints were coefficient of friction (COF), wear scar diameter (WSD), and comparative wear-rate index K. WSD was treated as the primary wear metric because it was directly measured from the wear scars of the three lower balls after testing using optical microscopy in accordance with ASTM

D4172-type evaluation procedures. Wear volume was estimated using the standard spherical-cap geometry of the wear scar, and K was calculated by normalizing the estimated wear volume with respect to applied load and sliding distance. The calculated K values were therefore used as comparative indicators for ranking formulation performance under identical test conditions. For transparency, the geometric basis for the wear-volume estimate was as follows:

$$h = R - \sqrt{(R^2 - (d/2)^2)} \quad (1)$$

$$V = \pi h^2 (3R - h)/3 \quad (2)$$

$$K = V/(F\,L) \quad (3)$$

where d is the mean WSD of the three lower balls, R = 6.35 mm is the ball radius, V is the spherical-cap wear volume, F is the applied load, and L is the effective sliding distance used in the tester software [21,22]. The reported K values in are used only as a comparative wear-rate index under identical test conditions, not as transferable absolute wear constants.

After testing, representative worn surfaces were examined by SEM at 15 kV. EDS targeted Ti, Mo, S, O, and Fe to determine whether additive-associated elements were present in the wear track and whether substrate exposure differed among samples. SEM/EDS cannot identify chemical bonding states or confirm tribochemical reactions; therefore, are interpreted as qualitative morphology and elemental evidence only. Direct confirmation of tribofilm chemistry would require XPS, Raman spectroscopy, TEM, AFM, or related surface-chemistry methods.

2.5 Statistical analysis

All data are reported as mean ± standard deviation from three independent measurements. Formulation effects were evaluated using one-way analysis of variance (ANOVA) at a significance level of $\alpha = 0.05$, followed by Tukey honestly significant difference (HSD) multiple-comparison analysis when the omnibus ANOVA result was significant. Tukey HSD was selected because it controls the family-wise Type I error rate during pairwise comparison of multiple formulations. Prior to ANOVA, the datasets were screened for consistency of variance and absence of abnormal outliers based on residual distribution and replicate variability. Because n = 3 per formulation provides limited statistical power for formal normality assessment, statistical interpretation was based not only on p-values but also on practical effect size, percentage change relative to BF, and overlap of Tukey grouping categories. WSD was treated as the primary wear endpoint because it was directly measured experimentally, whereas comparative wear-rate values were calculated from geometrically estimated wear volume normalized by applied load and sliding distance. The compact-letter Tukey groupings are presented in Table 2. K denotes the comparative wear-rate index.

Table 2. Tukey HSD compact-letter displays.

Sample	Apparent zeta potential	SI at 30 d	SI at 60 d	COF	WSD	K
BF	-	-	-	A	A	A
T05	A	B	A	B	B	B
M05	B	C	B	C	CD	C
H7525	BC	CD	BC	C	DE	C
H5050	BCD	DEF	CDE	D	EF	D
H2575	CD	EF	DE	E	F	D
H2575-0025	B	CD	BC	C	CD	C
H2575-0050	D	F	E	E	F	D
H2575-0075	BC	DE	BCD	D	EF	D
H2575-0100	A	A	A	B	BC	B

3. RESULTS AND DISCUSSION

3.1 Physicochemical and rheological behavior

The added base-fluid data show that the methyl-ester matrix was dominated by monounsaturated FAMEs, especially methyl oleate, with a substantial methyl linoleate fraction. This composition supports the interpretation of the fluid as a polar ester base capable of boundary adsorption, while the 180 d increase in acid number, water content, and peroxide value and the decrease in oxidation stability indicate progressive hydrolytic and oxidative degradation during storage. Consequently, the nanoparticle optimum should be interpreted for the characterized batch rather than assumed for severely aged base fluids or other independently prepared PPME:WCOME batches.

Table 3. Physicochemical and rheological properties of the biodiesel-derived tribofluids.

Sample	Density at 40 °C (kg/m^3)	KV at 40 °C (mm^2/s)	KV at 100 °C (mm^2/s)	Selected model R^2
BF	874.2 ± 1.1	4.68 ± 0.04	1.55 ± 0.02	0.995
T05	875.1 ± 1.0	4.82 ± 0.05	1.57 ± 0.02	0.992
M05	874.9 ± 1.2	4.76 ± 0.04	1.56 ± 0.02	0.995
H7525	875.0 ± 1.1	4.74 ± 0.04	1.56 ± 0.02	0.996
H5050	875.3 ± 1.0	4.73 ± 0.04	1.56 ± 0.02	0.997
H2575	875.4 ± 1.0	4.71 ± 0.03	1.56 ± 0.01	0.998
H2575-0025	875.0 ± 1.1	4.72 ± 0.04	1.56 ± 0.02	0.996
H2575-0050	875.2 ± 1.0	4.70 ± 0.03	1.56 ± 0.01	0.999
H2575-0075	875.6 ± 1.1	4.79 ± 0.05	1.57 ± 0.02	0.996
H2575-0100	876.1 ± 1.3	4.91 ± 0.06	1.59 ± 0.02	0.989

Table 3 shows that nanoparticle addition had little effect on density but produced a modest formulation-dependent change in low-temperature viscosity. Density at 40 °C varied only from 874.2 ± 1.1 kg/m3 for BF to 876.1 ± 1.3 kg/m3 for H2575-0100, and the ANOVA result was not significant. In contrast, KV at 40 °C increased from 4.68 ± 0.04 mm^2/s for BF to 4.91 ± 0.06 mm^2/s for H2575-0100. The H2575 and H2575-0050 formulations remained close to BF at 4.71 ± 0.03 and 4.70 ± 0.03 mm^2/s, respectively. This indicates that the 0.05 wt.% 25:75 hybrid preserved low-temperature flow more effectively than the overloaded 0.10 wt.% formulation. KV at 100 °C remained narrowly clustered between 1.55 and 1.59 mm^2/s and was not significant by ANOVA. Because all measured KV at 100 °C values were below the ASTM D2270-24 applicability threshold, viscosity index was not reported.

3.2 Dispersion stability and selection of the hybrid composition

Table 4 and Figure 2 show a clear stability trend from single-particle systems to MoS_2-rich hybrids. In the screening series, apparent zeta potential became more negative from T05 (-32.4 ± 1.6 mV) to H2575 (-44.1 ± 1.2 mV). At the same time, SI at 30 d decreased from 3.8 ± 0.3% for T05 to 1.4 ± 0.1% for H2575, and SI at 60 d decreased from 6.5 ± 0.5% to 2.8 ± 0.2%. These combined electrokinetic and settling trends indicate improved relative dispersion stability when the hybrid contained a higher MoS_2 fraction.

Table 4. Stability metrics for the biodiesel-derived tribofluids.

Sample	Apparent zeta potential (mV)	SI at 30 d (%)	SI at 60 d (%)
BF	NA	NA	NA
T05	-32.4 ± 1.6	3.8 ± 0.3	6.5 ± 0.5
M05	-38.7 ± 1.4	2.7 ± 0.2	4.8 ± 0.4
H7525	-40.8 ± 1.5	2.3 ± 0.2	4.1 ± 0.3
H5050	-42.6 ± 1.3	1.8 ± 0.2	3.4 ± 0.3
H2575	-44.1 ± 1.2	1.4 ± 0.1	2.8 ± 0.2
H2575-0025	-39.8 ± 1.4	2.2 ± 0.2	3.9 ± 0.3
H2575-0050	-45.7 ± 1.1	1.2 ± 0.1	2.5 ± 0.2
H2575-0075	-41.0 ± 1.5	2.0 ± 0.2	3.8 ± 0.3
H2575-0100	-34.2 ± 1.7	4.6 ± 0.4	7.3 ± 0.5

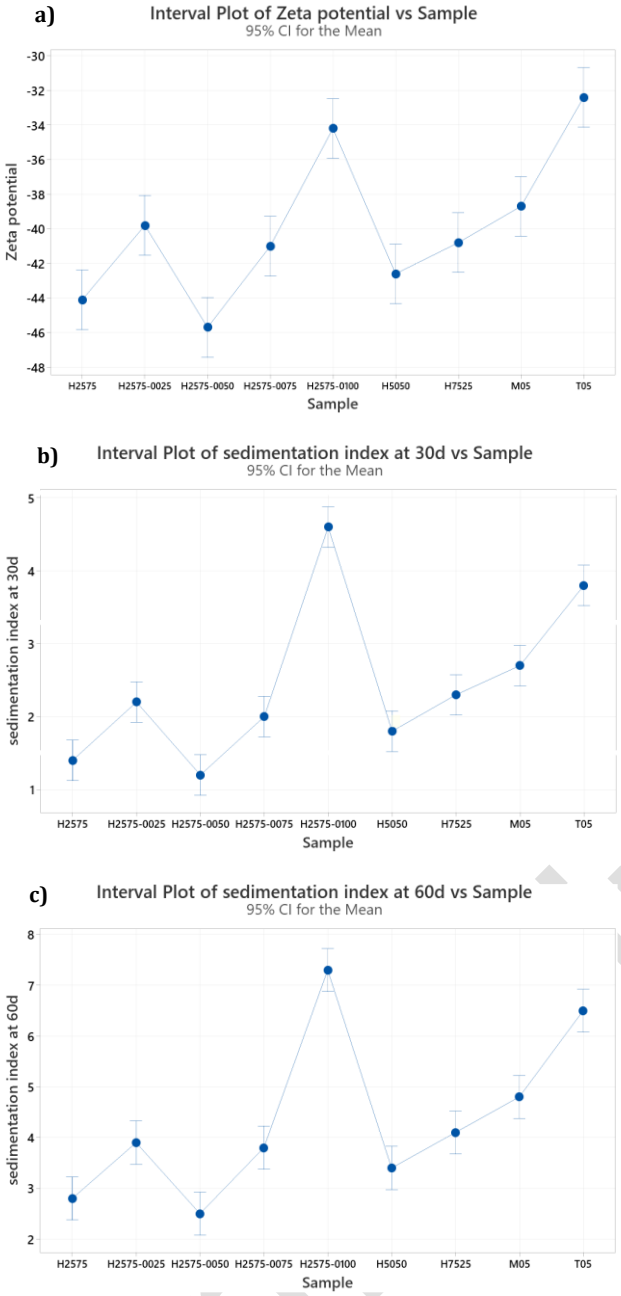

Fig. 2. Stability characteristics of the biodiesel-derived tribofluids: (a) apparent zeta potential, (b) sedimentation index at 30 d, and (c) sedimentation index at 60 d.

The loading series identified 0.05 wt.% as the most stable tested loading for the 25:75 hybrid. H2575-0050 reached the most negative apparent zeta potential (-45.7 ± 1.1 mV) and the lowest sedimentation indices at 30 d (1.2 ± 0.1%) and 60 d (2.5 ± 0.2%). Reducing the loading to 0.025 wt.% weakened the stability, while increasing the loading to 0.075 and especially 0.10 wt.% deteriorated it. H2575-0100 showed a less negative apparent zeta potential (-34.2 ± 1.7 mV) and higher SI values of 4.6 ± 0.4% at 30 d and 7.3 ± 0.5% at 60 d. This deterioration is consistent with agglomeration exceeding the steric stabilization capacity of the fixed Span 80 concentration, although agglomerate size was not measured directly.

The formulation effect was statistically significant for apparent zeta potential, SI at 30 d, and SI at 60 d. The compact-letter groupings in Table 2 show that H2575 and H2575-0050 belong to the strongest stability groups, but they should be interpreted as two independent preparations at the same nominal composition rather than as evidence that H2575-0050 is significantly better than H2575. The apparent zeta-potential values are not used as absolute non-aqueous stability constants; instead, the conclusion is based on agreement between apparent electrokinetic ranking, sedimentation behavior, and the tribological trends discussed below.

3.3 Tribological screening: role of nanoparticle identity and hybrid ratio

The particle-free base fluid produced the highest friction and wear, with COF of 0.086 ± 0.002, WSD of 0.71 ± 0.02 mm, and a comparative wear-rate index of 5.20 ± 0.15 × 10^{-6} mm^3/N.m Table 5 and Figure 3. Adding TiO_2 alone lowered these values to 0.071, 0.62 mm, and 4.40 × 10^{-6} mm^3/N.m, while MoS_2 alone further reduced them to 0.064, 0.58 mm, and 3.90 × 10^{-6} mm^3/N.m. The larger improvement with MoS_2 is consistent with its layered low-shear structure, but this study did not directly verify tribochemical bonding or exfoliation in the contact [12,13].

The hybrid systems gave the lowest friction and wear values in the screening stage. As the MoS_2 fraction increased from H7525 to H5050 and H2575 at 0.05 wt.%, COF, WSD, and the wear-rate index decreased progressively. H2575 reached a COF of 0.050 ± 0.001, WSD of 0.52 ± 0.01 mm, and wear-rate index of 3.20 ± 0.09 × 10^{-6} mm^3/N.m. Relative to BF, these values represent reductions of 41.9%, 26.8%, and 38.5%, respectively. The data support a composition-dependent hybrid benefit, but the term synergy is used cautiously because direct tribochemical or nanoscale contact-zone evidence was not obtained.

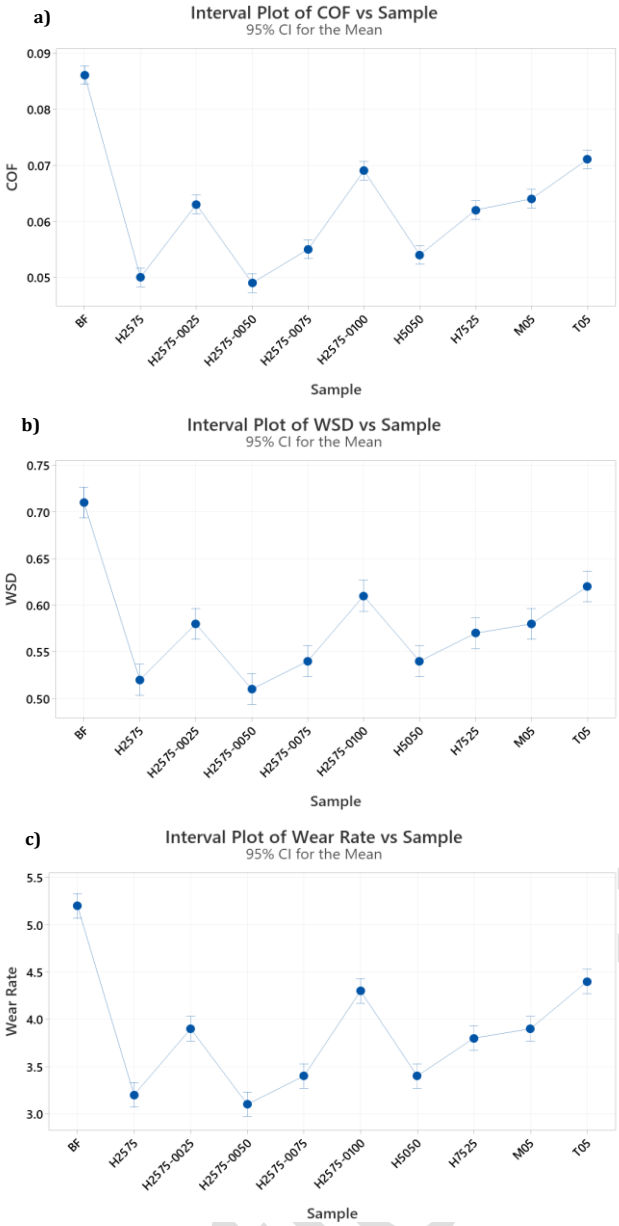

Fig. 3. Tribological performance of the biodiesel-derived tribofluids: (a) coefficient of friction, (b) wear scar diameter, and (c) comparative wear-rate index.

3.4 Loading optimization of the 25:75 TiO_2:MoS_2 hybrid

Within the 25:75 hybrid family, Table 5 and Figure 4 show a non-monotonic loading response. At 0.025 wt.% (H2575-0025), the additive improved performance relative to BF but did not reach the best response. The independent 0.05 wt.% batch (H2575-0050) reproduced the lowest measured COF (0.049 ± 0.001), WSD (0.51 ± 0.01 mm), and wear-rate index ($3.10 \pm 0.08 \times 10^{-6}$ mm^3/N.m). Increasing the loading to 0.075 wt.% partially reduced the benefit, and 0.10 wt.% caused a clear deterioration, with COF, WSD, and wear-rate index increasing to 0.069 ± 0.002, 0.61 ± 0.02 mm, and $4.30 \pm 0.12 \times 10^{-6}$ mm^3/N.m, respectively.

The 0.05 wt.% minimum suggests a balance between particle availability and dispersion quality. At low loading, the additive supply to the contact may have been insufficient for continuous surface coverage. At high loading, the sedimentation and apparent zeta-potential data indicate a higher probability of particle-particle interaction and agglomeration; such agglomerates can interrupt layer continuity and act as abrasive third bodies. Because particle-size distribution after storage and after testing was not measured, this explanation remains a proposed mechanism supported indirectly by stability, friction/wear, and SEM/EDS trends. Comparable intermediate-loading optima have been reported for other nanolubricants and hybrid systems [13-15,23].

Table 5. Tribological performance under four-ball test conditions:
(a) Friction response.

Sample	COF (mean ± SD)	COF reduction vs BF (%)
BF	0.086 ± 0.002	-
T05	0.071 ± 0.002	17.4
M05	0.064 ± 0.001	25.6
H7525	0.062 ± 0.001	27.9
H5050	0.054 ± 0.001	37.2
H2575	0.050 ± 0.001	41.9
H2575-0025	0.063 ± 0.001	26.7
H2575-0050	0.049 ± 0.001	43.0
H2575-0075	0.055 ± 0.001	36.0
H2575-0100	0.069 ± 0.002	19.8

(b) Wear response.

Sample	WSD (mm)	WSD reduction vs BF (%)	K (× 10^{-6} mm^3/N·m)	K reduction vs BF (%)
BF	0.71 ± 0.02	-	5.20 ± 0.15	-
T05	0.62 ± 0.02	12.7	4.40 ± 0.13	15.4
M05	0.58 ± 0.01	18.3	3.90 ± 0.11	25.0
H7525	0.57 ± 0.01	19.7	3.80 ± 0.10	26.9
H5050	0.54 ± 0.01	23.9	3.40 ± 0.09	34.6
H2575	0.52 ± 0.01	26.8	3.20 ± 0.09	38.5
H2575-0025	0.58 ± 0.01	18.3	3.90 ± 0.10	25.0
H2575-0050	0.51 ± 0.01	28.2	3.10 ± 0.08	40.4
H2575-0075	0.54 ± 0.01	23.9	3.40 ± 0.09	34.6
H2575-0100	0.61 ± 0.02	14.1	4.30 ± 0.12	17.3

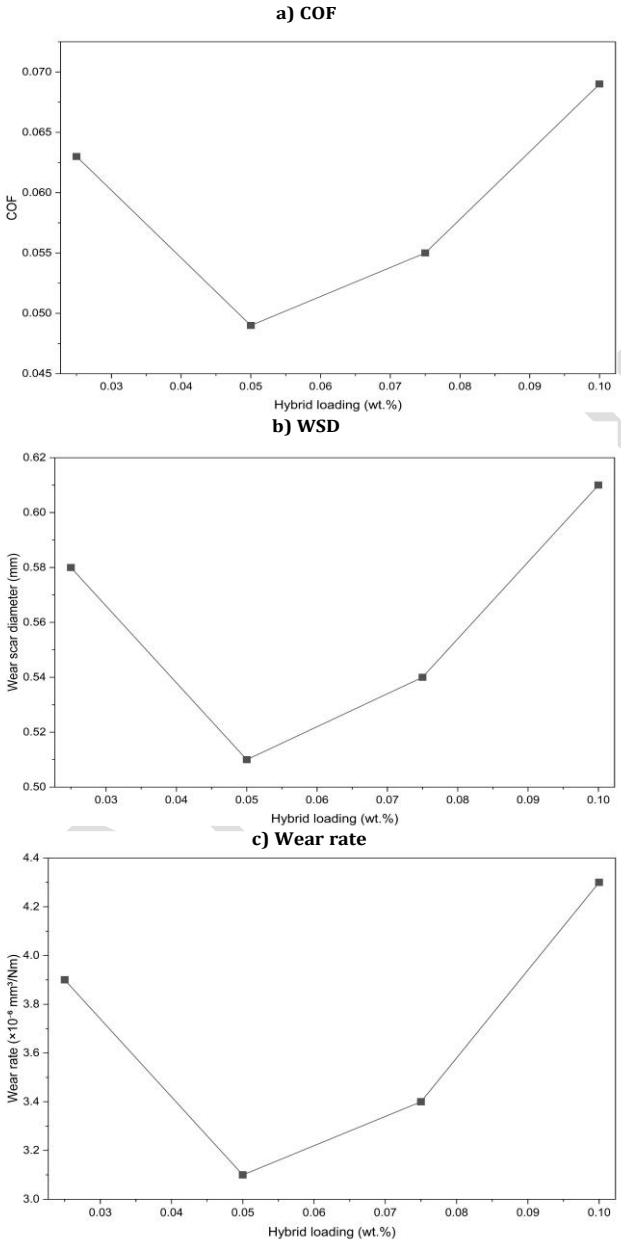

Fig. 4. Effect of total hybrid loading on the tribological response of the 25:75 TiO_2:MoS_2 system: (a) COF, (b) WSD, and (c) comparative wear-rate index.

3.5 Statistical interpretation and multiple-comparison results

Table 6 consolidates the omnibus ANOVA results. Density at 40 °C and KV at 100 °C were not significantly affected by formulation, whereas KV at 40 °C, all stability metrics, COF, WSD, and the wear-rate index were significant. The practical interpretation is that the additive package mainly changed dispersion stability and boundary-contact behavior, while density and high-temperature kinematic viscosity remained essentially unchanged within the tested matrix. The compact-letter displays in Table 2 identify the pairwise structure without repeating p-values throughout the text. H2575 and H2575-0050 share the lowest COF and WSD groups, indicating that the independent 0.05 wt.% preparation reproduced the screening-stage result rather than improving it significantly. The wear-rate-index grouping is broader because H5050 and H2575-0075 overlap statistically with the lowest group. Therefore, claims are based on both statistical grouping and practical effect sizes relative to BF, not on p-values alone.

3.6 SEM/EDS evidence and mechanistic interpretation

The SEM/EDS evidence in Table 7 and Figures 5 and 6 is consistent with the friction and wear ranking but remains qualitative. BF showed deep grooves and severe ploughing with Fe-, O-, and C-dominant signals, indicating substantial substrate exposure. T05 and M05 showed less severe wear features: Ti/O-associated signals were detected for T05, while Mo/S-associated signals were detected for M05. The hybrid samples showed progressively smoother tracks and mixed Ti/Mo/S/O signals, with H2575 and H2575-0050 giving the most uniform surface evidence among the tested formulations.

Table 6. Summary of one-way ANOVA results for key response variables.

Metric	F statistic	p-value
Density at 40 °C	F (9,20) = 0.612	0.773
KV at 40 °C	F (9,20) = 7.652	< 0.001
KV at 100 °C	F (9,20) = 1.020	0.458
Apparent zeta potential	F (8,18) = 27.944	< 0.001
SI at 30 d	F (8,18) = 70.963	< 0.001
SI at 60 d	F (8,18) = 63.886	< 0.001
COF	F (9,20) = 199.316	< 0.001
WSD	F (9,20) = 54.667	< 0.001
Wear rate	F (9,20) = 106.461	< 0.001

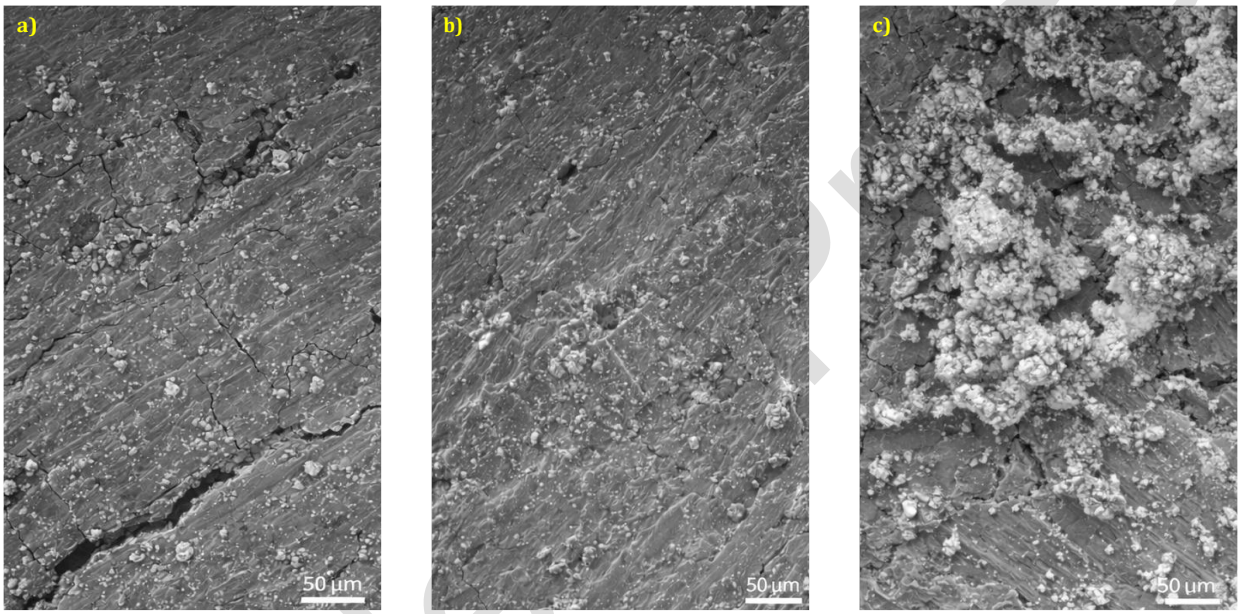

Fig. 5. SEM surface analysis of representative wear scars: (a) BF, (b) H2575-0050, and (c) H2575-0100.

Table 7. Surface morphology and protective-layer evidence from SEM/EDS analysis.

Sample	SEM observation	EDS within wear track	Interpretation
BF	Deep grooves and severe ploughing	Fe, O, and C dominant	No additive layer; high Fe exposure
T05	Moderate grooves and partial smoothing	Ti, O, Fe, and C	Ti/O deposits; partial smoothing
M05	Reduced ploughing and fewer debris particles	Mo, S, Fe, and C	Mo/S deposits; less ploughing
H7525	Smoother track with shallow grooves	Ti, Mo, S, O, Fe, and C	Mixed Ti/Mo/S/O deposits
H5050	Smooth track and compacted layer	Ti, Mo, S, O, Fe, and C	More continuous mixed layer
H2575	Minimal grooves and almost no loose debris	Strong Ti, Mo, S, and O signals	Uniform screening-stage signal
H2575-0025	Good smoothing but comparatively thin layer	Ti, Mo, S, O, Fe, and C detectable	Partial mixed layer
H2575-0050	Smoothest track and most compact continuous layer	Strong and more uniform Ti/Mo/S signals	Most uniform additive signal
H2575-0075	Good layer with local agglomerate patches	Ti, Mo, and S present but less uniform	Heterogeneous layer
H2575-0100	Patchy layer, renewed grooves, and loose debris	Non-uniform Ti/Mo/S distribution with relatively stronger Fe exposure	Patchy layer; Fe re-exposure

H2575-0050 produced the smoothest representative track and the most uniform Ti/Mo/S-associated EDS response (Figures 5 and 6). Compared with H2575-0100, it showed less renewed grooving, less loose debris, and weaker evidence of substrate re-exposure. In contrast, H2575-0100 displayed a patchier surface with non-uniform Ti/Mo/S distribution and relatively stronger Fe exposure. This supports the interpretation that excessive loading reduced surface-layer continuity, probably through agglomeration and third-body abrasion. Because no XPS, Raman, TEM, or AFM measurements were performed, the manuscript avoids assigning specific chemical bonding states or claiming confirmed tribochemical film formation.

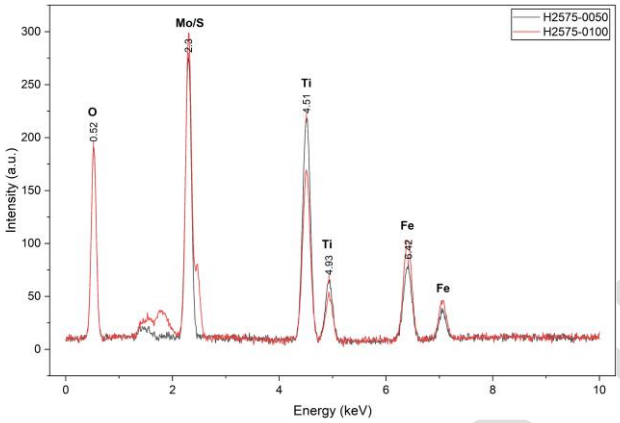

Fig. 6. Comparative EDS spectra of the wear tracks lubricated by H2575-0050 and H2575-0100.

3.7 Comparison with literature, industrial relevance, and limitations

The 43.0% friction reduction and 28.2% WSD reduction obtained for H2575-0050 are comparable with reported improvements for other nanoadditive systems, but direct numerical comparison must be made cautiously because base oils, surface pairs, loads, temperatures, test durations, and dispersion protocols differ. For example, TiO_2/MoS_2 hybrid additives in SAE 10W-30 oil have been reported to reduce friction by about 40% under four-ball testing [14], while MoS_2- and WS_2-based castor-oil nanolubricants have shown friction reductions of the same general order and WSD reductions near 20-25% [13]. Recent low-viscosity oil studies also show that MoS_2 can produce large friction and wear reductions when surface chemistry is verified by Raman or roughness mapping [23]. The present contribution differs by using a methyl-ester blend derived from a non-edible seed oil and waste cooking oil, and by linking stability, viscosity, four-ball results, and SEM/EDS evidence within one formulation matrix.

From an industrial perspective, the low additive concentration, use of waste-derived and non-edible feedstocks, unchanged density and KV at 100 °C, and now-reported base-fluid FAME and fuel-quality data are favorable. However, the work remains a laboratory screening study. The storage data showed increasing acid number, water content, and peroxide value with decreasing oxidation stability over 180 d, so practical deployment would require control of base-fluid ageing as well as batch-to-batch characterization, oxidative and thermal aging tests, compatibility with seals and metals, filtration and storage evaluation, durability testing under longer sliding periods, load-temperature mapping, and comparison with commercial biodegradable and mineral lubricant benchmarks. These needs are listed as future work because the present data were limited to one ASTM D4172-type condition and qualitative SEM/EDS surface analysis.

4. CONCLUSION

Within the tested formulation window, a 25:75 TiO_2:MoS_2 hybrid at 0.05 wt.% gave the best batch-specific balance of storage stability and four-ball tribological performance in the 50:50 PPME:WCOME base fluid. In the screening stage, the 25:75 hybrid outperformed the single-particle TiO_2 and MoS_2 formulations. In the loading stage, the independently prepared H2575-0050 formulation reproduced the same response rather than showing a statistically significant improvement over the screening-stage H2575 sample. H2575-0050 showed an apparent zeta potential of -45.7 ± 1.1 mV, sedimentation indices of 1.2 ± 0.1% at 30 d and 2.5 ± 0.2% at 60 d, COF of 0.049 ± 0.001, WSD of 0.51 ± 0.01 mm, and comparative wear-rate index of $3.10 \pm 0.08 \times 10^{-6}$ mm^3/N.m. Relative to BF, COF, WSD, and the wear-rate index decreased by 43.0%, 28.2%, and 40.4%, respectively, while density and KV at 100 °C remained statistically unchanged.

SEM/EDS supported the performance ranking by showing smoother wear tracks and more uniform Ti/Mo/S-associated signals for H2575-0050 than for the overloaded H2575-0100

formulation. The mechanistic interpretation is deliberately limited to additive-associated surface material, reduced substrate exposure, and probable loss of layer continuity at excessive loading. Direct tribochemical film formation was not verified. The apparent zeta-potential values should be treated as relative non-aqueous stability metrics. The base fluid was characterized in terms of FAME distribution, acid number, water content, oxidation stability, peroxide value, ester purity, and storage-quality change; nevertheless, the reported optimum should not be generalized to other biodiesel batches or aged fluids without independent batch characterization and validation under broader load-temperature and durability conditions.

REFERENCES

[1] J. K. Mannekote, S. V. Kailas, K. Venkatesh, and N. Kathyayini, "Environmentally friendly functional fluids from renewable and sustainable sources—A review," *Renewable and Sustainable Energy Reviews*, vol. 81, pp. 1787–1801, Jan. 2018, doi: 10.1016/j.rser.2017.05.274.

[2] R. Shah, A. Martini, M. Woydt, and H. Wong, "Green Tribology," *Tribology in Industry*, vol. 42, no. 4, pp. 592–596, Dec. 2020, doi: 10.24874/ti.987.10.20.11.

[3] K. Holmberg and A. Erdemir, "Influence of tribology on global energy consumption, costs and emissions," *Friction*, vol. 5, no. 3, pp. 263-284, 2017, doi: 10.1007/s40544-017-0183-5.

[4] M. Khadem, W.-B. Kang, and D.-E. Kim, "Green Tribology: A Review of Biodegradable Lubricants-Properties, Current Status, and Future Improvement Trends," *International Journal of Precision Engineering and Manufacturing-Green Technology*, vol. 11, no. 2, pp. 565-583, 2024, doi: 10.1007/s40684-023-00556-x.

[5] D. C. M. Ribeiro, A. Ramalho, A. C. Serra, and J. Coelho, "Biolubricants Based on Epoxidized Vegetable Oils: A Review on Chemical Modifications, Tribological Properties, and Sustainability," *Lubricants*, vol. 13, no. 12, art. 510, 2025, doi: 10.3390/lubricants13120510.

[6] G. Oncu and E. Durak, "Utilization of waste vegetable oil methyl esters as lubricant oil," *Proceedings of the Institution of Mechanical Engineers, Part J: Journal of Engineering Tribology*, vol. 235, no. 10, pp. 2144–2154, Oct. 2021, doi: 10.1177/1350650120987930.

[7] A. K. Paul, V. B. Borugadda, and V. V. Goud, "In-Situ Epoxidation of Waste Cooking Oil and Its Methyl Esters for Lubricant Applications: Characterization and Rheology," *Lubricants*, vol. 9, no. 3, art. 27, Mar. 2021, doi: 10.3390/lubricants9030027.

[8] N. W. M. Zulkifli, S. S. N. Azman, M. A. Kalam, H. H. Masjuki, R. Yunus, and M. Gulzar, "Lubricity of bio-based lubricant derived from different chemically modified fatty acid methyl ester," *Tribology International*, vol. 93, pp. 555-562, Jan. 2016, doi: 10.1016/j.triboint.2015.03.024.

[9] A. E. Atabani, A. S. Silitonga, H. C. Ong, T. M. I. Mahlia, H. H. Masjuki, I. A. Badruddin, and H. Fayaz, "Non-edible vegetable oils: A critical evaluation of oil extraction, fatty acid compositions, biodiesel production, characteristics, engine performance and emissions production," *Renewable and Sustainable Energy Reviews*, vol. 18, pp. 211–245, Feb. 2013, doi: 10.1016/j.rser.2012.10.013.

[10] U. N. Annal, M. S. A. J. Bosco, G. Raman, P. S. M. Kumar, M. Afzal, P. Khurana, and M. Durai, "Ultrasound-assisted biodiesel production from Peltophorum pterocarpum oil: A comparative analysis of prediction accuracy between RSM and ANFIS," *Biocatalysis and Agricultural Biotechnology*, vol. 65, art. 103545, 2025, doi: 10.1016/j.bcab.2025.103545.

[11] C. Birleanu, M. Pustan, M. Cioaza, A. Molea, F. Popa, and G. Contiu, "Effect of TiO_2 nanoparticles on the tribological properties of lubricating oil: an experimental investigation," *Scientific Reports*, vol. 12, art. 5201, 2022, doi: 10.1038/s41598-022-09245-2.

[12] Z. Lu, Q. Lin, Z. Cao, W. Li, J. Gong, Y. Wang, K. Hu, and X. Hu, "MoS_2 Nanomaterials as Lubricant Additives: A Review," *Lubricants*, vol. 11, no. 12, art. 527, Dec. 2023, doi: 10.3390/lubricants11120527.

[13] J. Srivastava, T. Nandi, and R. K. Trivedi, "Experimental Investigations on Thermophysical, Tribological and Rheological Properties of MoS_2 and WS_2 Based Nanolubricants with Castor Oil as Base Lubricant," *Tribology in Industry*, vol. 45, no. 4, pp. 591–603, Dec. 2023, doi: 10.24874/ti.1472.04.23.07.

[14] L. B. Abhang, S. A. Kale, A. Sambare, and S. Katore, "Experimental study on engine oil blended with TiO_2 & MoS_2 hybrid nanoparticles," *Tribologia – Finnish Journal of Tribology*, vol. 42, no. 1–2, pp. 45–63, 2025, doi: 10.30678/fjt.157308.

[15] N. Hamzan, I. A. Zakaria, J. Abdul Ghani, N. H. Abdul Halim, W. A. Wan Hamzah, Z. H. Solihin, and A. A. Ahmad, "The SiO_2:TiO_2 hybrid biodegradable nanolubricant for sustainable machining: The stability, thermo-physical and tribology perspectives," *Tribology International*, vol. 207, art. 110614, 2025, doi: 10.1016/j.triboint.2025.110614.

[16] D. J. Pochapski, C. C. dos Santos, G. W. Leite, S. H. Pulcinelli, and C. V. Santilli, "Zeta Potential and Colloidal Stability Predictions for Inorganic Nanoparticle Dispersions: Effects of Experimental Conditions and Electrokinetic Models on the Interpretation of Results," *Langmuir*, vol. 37, no. 45, pp. 13379–13389, Nov. 2021, doi: 10.1021/acs.langmuir.1c02056.

[17] ASTM International, *Standard Test Method for Density, Relative Density, and API Gravity of Liquids by Digital Density Meter*, ASTM D4052-18, ASTM International, West Conshohocken, PA, 2018, doi: 10.1520/D4052-18.

[18] ASTM International, *Standard Test Method for Kinematic Viscosity of Transparent and Opaque Liquids and Calculation of Dynamic Viscosity*, ASTM D445-21e1, ASTM International, West Conshohocken, PA, 2021, doi: 10.1520/D0445-21E01.

[19] ASTM International, *Standard Practice for Calculating Viscosity Index from Kinematic Viscosity at 40 °C and 100 °C*, ASTM D2270-24, ASTM International, West Conshohocken, PA, 2024, doi: 10.1520/D2270-24.

[20] ASTM International, *Standard Test Method for Wear Preventive Characteristics of Lubricating Fluid — Four-Ball Method*, ASTM D4172-25, ASTM International, West Conshohocken, PA, 2025, doi: 10.1520/D4172-25.

[21] M. S. Wright, V. K. Jain, and C. S. Saba, "Wear rate calculation in the four-ball wear test," *Wear*, vol. 134, no. 2, pp. 321–334, Nov. 1989, doi: 10.1016/0043-1648(89)90134-8.

[22] A. Bos, "Wear in the four-ball apparatus: relationship between the displacement of the upper ball and the diameter of the wear scars on the lower balls," *Wear*, vol. 41, no. 1, pp. 191–194, Jan. 1977, doi: 10.1016/0043-1648(77)90201-0.

[23] J. M. Liñeira del Río, C. M. C. G. Fernandes, and J. H. O. Seabra, "Tribological Improvement of Low-Viscosity Nanolubricants: MoO_3, MoS_2, WS_2 and WC Nanoparticles as Additives," *Lubricants*, vol. 12, no. 3, art. 87, 2024, doi: 10.3390/lubricants12030087.

Abbreviations

AISI - American Iron and Steel Institute
ANOVA - Analysis of variance
ASTM - American Society for Testing and Materials
BF - base fluid
COF - coefficient of friction
EDS - energy-dispersive X-ray spectroscopy
FAME - fatty acid methyl ester
GC-FID - gas chromatography with flame-ionization detection
HRC - Rockwell hardness, C scale
HSD - honestly significant difference
KOH - potassium hydroxide
KV - kinematic viscosity
MoS_2 - molybdenum disulfide
PPME - Peltophorum pterocarpum methyl ester
R_a - arithmetic average surface roughness
RMSE - root mean square error
R^2 - coefficient of determination
SD - standard deviation
SEM - scanning electron microscopy
SI - sedimentation index
TiO_2 - titanium dioxide
UV-Vis - ultraviolet-visible spectroscopy
WCO - waste cooking oil
WCOME - waste cooking oil methyl ester
WSD - wear scar diameter